EasyChair Preprint

№ 7826

Synthesis of a New Nanomaterial "Triphosphate of Niobium" Characterization and Advanced Structure Study Application: Improve Mechanical Strength of Implant and the Osteointegration Process

Mohamed Faoussi, Bouazza Tbib, Zakaria Kbiri and Salim Bounou

April 22, 2022

Synthesis of a New Nanomaterial "Triphosphate of Niobium" Characterization and Advanced Structure Study Application: Improve Mechanical Strength of Implant and the Osteointegration Process

Faoussi Mohamed*[1], Tbib Bouazza[2], Zakaria Kbiri[3] And Bounou Salim[1]

[1]: Euro-Mediterranean University, Health Science Laboratory, Fez, Morocco
[2]: Moulay Silman University, Nano-sciences and Modeling Laboratory, Khouribga, Morocco
[3]: University of Mohammed V, Rabat, Scientific Institute, BP 703, Av. Ibn Batouta, Agdal, Rabat, Morocco,
*m.faoussi@ueuromed.org

Abstract. Obtaining and maintaining implant stability are two essential conditions for the long-term functional success of bone-anchored prostheses. However, this initial stability also depends on other factors such as: the geometric shape of the implant, the clinician and the surgical protocol. After the primary healing, we have the secondary stability which is determined by the biological response to the surgical trauma, the patient's state of health, the healing conditions, the material of which the implant is made and its biocompatibility (physical, chemical properties and mechanical). In this work we synthesized a new nanomaterial "Niobium Triphosphate NbP_3O_{10}" by the solid-state method according to a well-defined thermal cycle (1000°C for 6 hours).
The objective is to make an advanced structural study of our nanomaterial in order to identify its physical characteristics. The purpose of our nanomaterial is to increase the mechanical resistance of our implant and improve bone healing by a surface coating. The characterization and identification of Niobium Triphosphate NbP3O10 was validated by three techniques: X-Ray diffraction; FT-IR Spectroscopy; X-ray fluorescence Spectrometry. A finite element modeling is made on Catia V5, by applying Von Mises constraints in order to calculate the deformation energy.

Keywords: Osseo-integration; Orthopedic; Nanomaterials; Implant Stability; Triphosphate; Mechanical Strength.

I Introduction

Nowadays, osseointegration is widely used in dental, orthopedic, maxillofacial and cancer surgery where defects pose serious functional and aesthetic problems.

The concept of osseointegration was defined by Per Ingvar Brånemark in 1965 as being a direct bone apposition on the implant surface (1), subsequently osseointegration took the name of "functional ankylosis" (2). It is characterized by direct structural and functional coaptation between living bone and the implant surface (3). It is the result of direct primary bone regeneration on the implant.

This process is reflected in two phases, or by two complementary stabilities: immediate stability of the implant after its surgical placement, this corresponds to “primary” or “mechanical” stability; this phase gradually decreases to be replaced by “secondary” or “biological” stability, which is determined by a well-defined biological process. (See Figure 1)

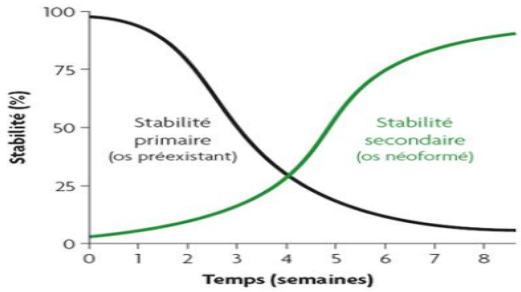

Fig. 1. Diagram of the progressive decrease in primary stability, responsible for the immobility of the implant and the increase in biological stability

1.1 Mechanical Stability (Primary Stability)

Primary stability represents the level of immobility of an implant after its surgical placement. It is a mechanistic criterion, which promotes bone healing and osseointegration. In the absence of satisfactory primary stability, the bone-implant interface may be the site of persistent micromovements. When they are too great, they lead to fibro-integration of the implant, synonymous with implant failure.

In this case, we have filed a national invention patent No. 41535, with the aim of improving primary stability. This work was accepted and approved by the Patent Department of OMPIC Morocco, on 16 May, 2018.

1.2 Secondary Stability (Biological Stability)

Secondary stability is a biological response to surgical trauma, through bone regeneration and remodeling.

This bone regeneration takes place in several stages (See Figure 2)

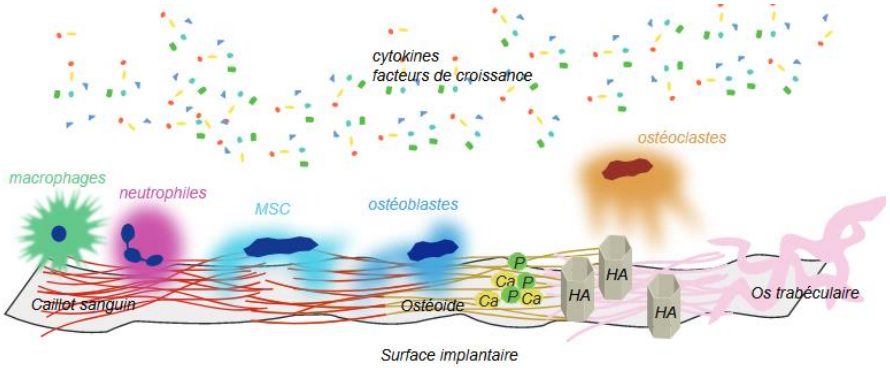

Fig. 2. The different stages of biological stability

- Initially, the alliance between the proteins of the inflammatory response (Ex: fibrogens) and the blood platelets, forms a network of fibrin, on which the cells necessary for bone remodeling can move.
- Then, chemical mediators are released, initiating a cascade of cellular activations starting with macrophages and neutrophils, which are responsible for cleaning the site, suppressing pathogens and managing inflammatory metabolism.
- The previously formed fibrin network also allows mesenchymal stem cells (MSC) to migrate to the site. These cells differentiate into osteoblasts, which will gradually replace the fibrin matrix with a collagen bone matrix. Calcium (Ca) and phosphate (P) ions are deposited on this collagen matrix to form hydroxyapatite (HA) crystals
- Finally, the osteoclasts will remodel this newly synthesized bone tissue and thus initiate a remodeling, in association with the osteoblasts which will remove small imperfections by filling in these resorptions to make the mature bone more resistant. (4)

To improve the bone healing, we have several determining factors that can lead to the success or failure of the osseointegration process, they are divided into three categories:

- **Patient-related factors**: the quality and quantity of a patient's soft and hard tissues are directly related to their state of health (cardiovascular disorders, endocrine disorders, etc.). Lifestyle habits (sport, alcohol, tobacco, etc.) are also factors that have a great influence on the biological response of the human body, following an implantology intervention.
- **Factors related to the surgical technique**: today, the surgeon has different surgical techniques to optimize primary stability, either by using screw systems, or systems with skeletal integration thanks to bone growth in a microporous structure of the implant.
- **Factors related to the implant**: mechanical strength, biocompatibility and surface condition of the implant.

In this work we are interested in the factors related to the implant, in particular the resistance to deformation and the surface condition, because they can significantly influence the success of the osseointegration process (5).

Indeed, the surface condition determines the possibility for the blood to cover the material very quickly, inducing good bone healing.

In addition, the wettability (wetting) designates on the one hand, the form that the blood takes on the surface of the implant (static wetting), and on the other hand, the behavior of the blood in contact with this surface. These behaviors arise from the interactions, which are determined by the surface energy. Therefore, the higher this energy, the greater the wettability.

Scientific research has shown that several parameters influence the surface energy as well as the wettability of the implant, such as: the roughness and the composition of the biomaterial used. Indeed, these authors have confirmed the link between the power of wettability and the adhesion of bone cells (6) (7) (8).

In this article we worked on the identification of a new nanomaterial "niobium triphosphate (NbP_3O_{10})". its characterization is made by three techniques: X-Ray diffraction, FT-IR Spectroscopy and X-ray Fluorescence Spectrometry. The usefulness of our nanomaterial is to promote the onsteointegration process thanks to an implant surface coating. In fact, bone contains about 85% of the body's phosphate. It intervenes to promote thermodynamically the biochemical reactions of bone anabolism. In addition, Niobium (Nb) is an alloying agent that imparts unique properties to materials to which it is added. Indeed, the addition of niobium to titanium gives it undeniable advantages, at the medical, economic and environmental level, because it increases the mechanical resistance of our implant, lightens it and makes it hypoallergenic. Thanks to its exceptional properties.

II Experimental

2.1 Synthesis of Niobium triphosphates NbP_3O_{10}

The precursors selected for synthesis were 99.999% Nb2O5 and 99.999% (NH4)2HPO4 (Aldrich). Niobium triphosphates were obtained by solid route according to the following reaction.

$$0.5Nb2O5+3(NH4)2HPO4 \longrightarrow NbP3O10 +xCO2+yNO2+zH2O +zO2$$

The stoichiometric proportions of the reactant mixtures being thoroughly ground in a mortar in order to obtain a homogeneous mixture facilitating vitrification are then introduced into a platinum crucible and then placed in an oven to undergo a decomposition treatment before melting. This preliminary cycle makes it possible to ensure the decomposition of the reactants and the gaseous releases occurring during the preceding reaction, namely H2O, NH3 from

155 °C and NO2 at 444 ° C.

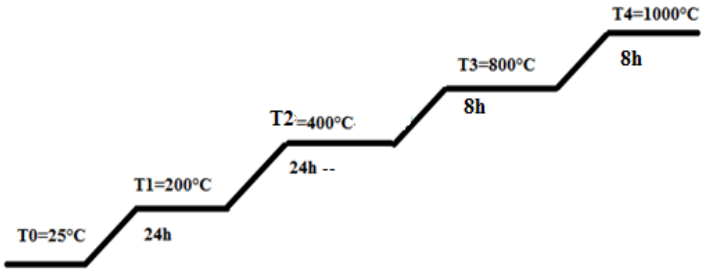

Fig. 3. Heat treatment cycle allowing the decomposition of the reagents

Fig. 4. Photograph of NbP_3O_{10} phosphates inside the alumina crucible at room temperature (25°C)

Fig. 5. Photograph of NbP_3O_{10} phosphates inside the alumina crucible at 400°C

Fig. 6. Photograph of NbP_3O_{10} phosphates inside the alumina crucible at 1000°C before grinding

Fig. 7. Photograph of NbP_3O_{10} phosphates inside the alumina crucible at 1000°C after grinding

2.2 Characterization of Niobium triphosphates NbP_3O_{10}

a) X-Ray diffraction study

X-ray powder pattern was carried out at room temperature using a diffractometer in the step scan mode (CuKα radiation, at a step value of 0.02°). X-ray analysis of the triphosphate de Niobium NbP_3O_{10} shows that this phase crystallizes in the Monoclinic system (Space Group: P 2/m) with the following unit cell parameters: a = 13.036 Å, b =11.3182 Å, c = 12.539 Å, α= γ =90°, β=117.903 ° and direct Cell Volume = 892.546 $Å^3$. For the sample a major peak is observed at about 20.86°. The obtained Rietveld coefficients are indication of a good concordance between the observed and calculated diagram profiles. The Figure 1 gives the observed, calculated and difference powder XRD profiles of triphosphate de Niobium NbP_3O_{10}. The Bragg positions are also indicated. Results of the structural refinement of triphosphate de Niobium NbP_3O_{10} are given in Table I.

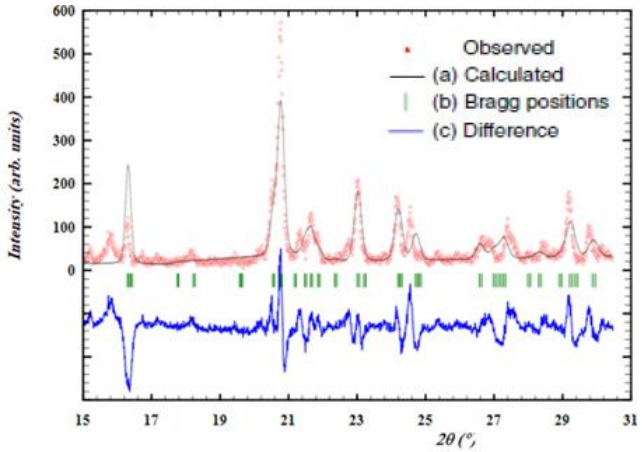

Fig. 8. Observed, calculated and difference powder XRD profiles of Niobium NbP_3O_{10}

The measurements are performed on (112) diffraction peak. The formed crystallite size of NbP_3O_{10} is calculated from the full width at half maximum (FWHM), of the (112) peak using Debye-Scherrer formula (9).

$$D = 0.9*\lambda / (\beta cos\theta)$$

Where D is the average crystallite size, β is the FWHM, λ is the wavelength of incident X-ray and θ is the angle of diffraction. The NbP_3O_{10} nanoparticles size was obtained in the above XRD pattern as 0.04 µm.

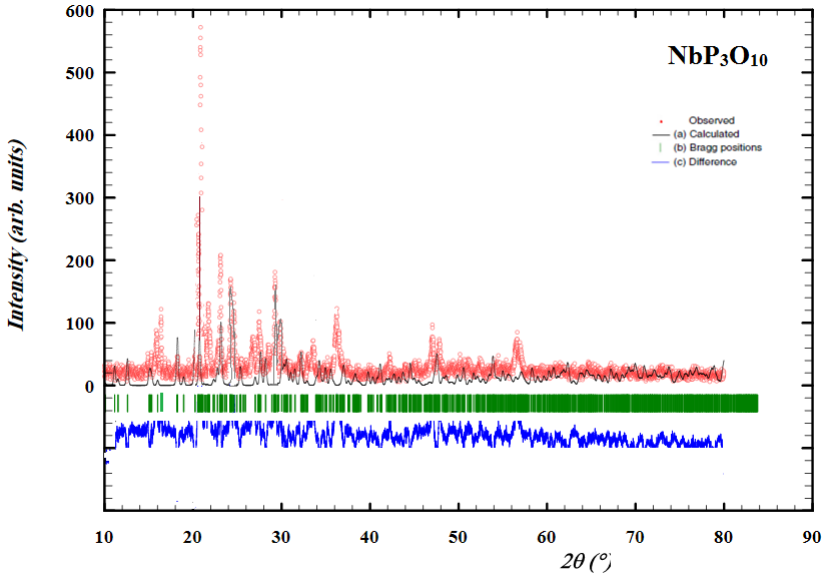

Fig. 9. Rietveld refinement spectrum of NbP_3O_{10} phase

Table 1: Results of the Rietveld refinement of NbP_3O_{10} phase

Formula	*NbP_3O_{10}*
Crystal system, S.G.	Monoclinic ,P 2/m
a (Å)	12.6557
b (Å)	8.778
c (Å)	8.2890
α= γ= (°)	*90°,*
β=	112.148
*Volume(*Å)	852.9109 Å^3
D(µm)	*0.04*
Rwp:	
Rexp:	*23.66*
X2	*25.45*
U	*-0.628621*
V	*0.567999*
W	*0.008911*

Table 2: The atomic positions of NbP_3O_{10}

Atoms	*x*	*y*	*z*
P1	0.08391	0.52639	0.35389
P2	0.06693	0.66691	0.44693
O1	0.13180	0.73996	0.54226
O 2	-0.09692	0.37166	-0.31623
O3	1.03124	0.22189	0.45211

O4	0.08568	0.29053	0.44544
O5	0.30278	0.68424	0.65010
Nb1	0.00000	0.00000	0.00000
Nb2	0.33180	0.54569	0.30643
Nb3	0.24892	0.95946	0.36682

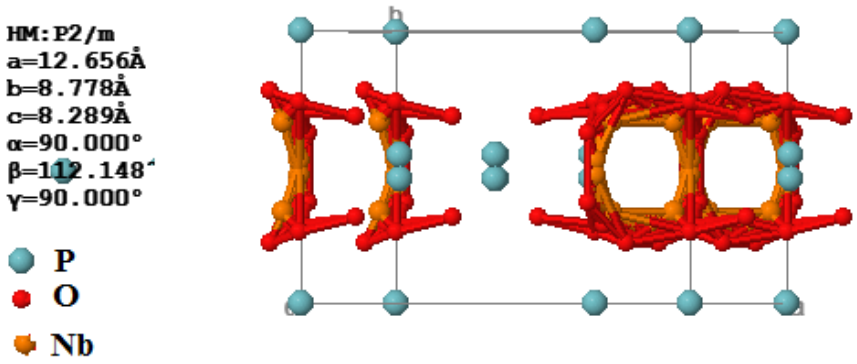

Fig. 10. Represent the cell of the structure NbP_3O_{10}

Table 3: Represents the values of energy during network vibration using Jmol

Time	Energy
10	9.883367
20	0.127799
30	-1.093610
40	-1.988347
50	-2.655187
60	-3.158434
70	-3.541973
80	-3.836669
90	-4.060002
100	-4.219768

b) FT-IR Spectroscopy

The vibrational study by infrared spectroscopy of triphosphates NbP_3O_{10} allows having a very fast structural information, in particular the identification of the various basic groupings forming phosphatic material. Indeed, the number and the distribution of the bands frequencies depend on local symmetry nature of the $P_3O_{10}^{5-}$ anion. The spectrum of Niobium NbP_3O_{10} compound (Figure 2) shows the existence of band around 954,5 cm^{-1} assigned with symmetric stretching vibration of the P-Ô-P Bridge. These bands are characteristic of triphosphates groups ($P_3O_{10}^{5-}$) In the 975-1300 cm^{-1} domain (10) (11), frequencies related to the symmetric and antisymmetric vibration modes of terminal $(PO_3)^{2-}$groups have

been evidenced. The bands around 400-700 cm^{-1} were assigned to the deformation and rocking modes of PO_3 groups (12). Furthermore, the existence of $\nu_s(PO_3)$ frequencies in the infrared spectrum indicates that $[P_3O_{10}]$ ring adopts a bent configuration.

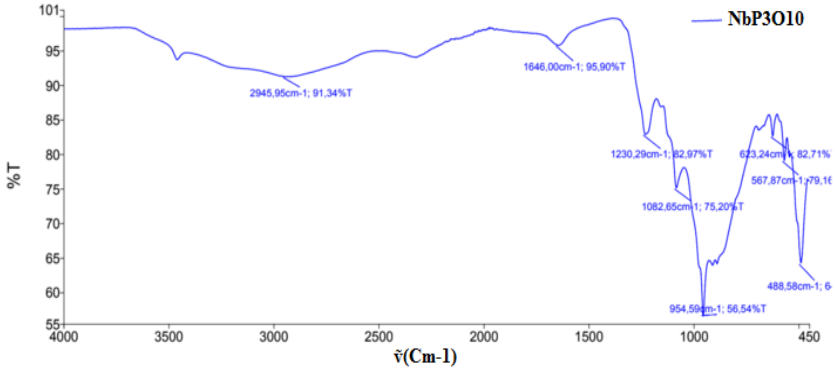

Fig. 11 The transmission spectra of Triphosphates NbP_3O_{10}

Table 4: Summarizes the band assignments for NbP_3O_{10}

Frequency value (cm^{-1})	Transmittance (%)	Assignment
2945 1648 1230,20 1082,65	91,34 95,90 82,97 75,20	$\nu_{as}PO_3$
954,50	56,54	ν_sPO_3
954,50	56,54	ν_{as}P-O-P
623,24 567,9 488,6	82,71 79,16 60,10	δPO_3 & ρPO_3

*ν= stretching vibration, *νs = symmetric stretching vibration, ν*as = asymmetric stretching vibration and *δ = wagging

c) X-ray fluorescence Spectrometry

The triphosphate of Niobium NbP_3O_{10} was characterize by the X-ray fluorescence figure 2, the optical phenomena are present, all the objects are characterized by the fluorescence, the fluorescence it is an optical phenomenon in numerous applications this phenomenon based on the emission of the light by a seen material that it was enlightened, we are interested in the specters of absorption, wavelengths are absorbed by the material, it absorbs many lights when we enlightened the material by the fluorescence we brought the energy of the materials which passed in an excited state, I think that this state is very unstable, on the other hand, the incited electrons are going to fall again on a fundamental state with the emission of the light, just a little energy is lost by said no transitions radioactive, the photon emitted by the possessed material less energy than the photon which served to excite, this observation participated in the mechanism of

interaction between the light and the material, the transfers of the energy between the light and the atoms of the material are made by discreet jump and its discreet energy, it is the science of the quantum mechanics. The specter of the X-rays accumulated during this process reveals a number of characteristic peaks. The energies of peaks allow us to identify the present elements in the sample whereas the intensities of peaks supply the relative concentration. As these transitions concern electrons strongly bound of the internal layers, the energies of the levels, and consequently the energies of the transitions, are essentially independent from the chemical state of the atom. The transitions between outer layers can have relatively big variations of the energies of emission, due to the effects in the band of valence, and thus by generating information of diverse nature. The same information is contained in the transitions X which have their origin in outer layers. The relatively high energy of the X-rays of emission allowed an actual analysis in volume of material, because the energy radiation has a bigger probability of transmission through the material without being absorbed. Several elements are present in the triphosphate of Niobium NbP_3O_{10}, who translate the relative absorption, these a linear combination of the concentrations as to present them in the table II. Both major elements are analyzed (Nb and P). Seventeen elements in tracks usually measured are it from pastilles. For other elements in tracks, in particular the elements of transition, spectral interferences can limit the dosage to samples presenting contents relatively more important. For elements in track, the limit of detection is generally 5 ppm, not taken into account here; elements in the table II are measurable with nearby limits of analysis of 10 ppm. All the values quoted here correspond to made measures "in routine" with the standard preparation and could be improved by changing the analytical process, or the treatment according to matrices, elements which we want to favor.

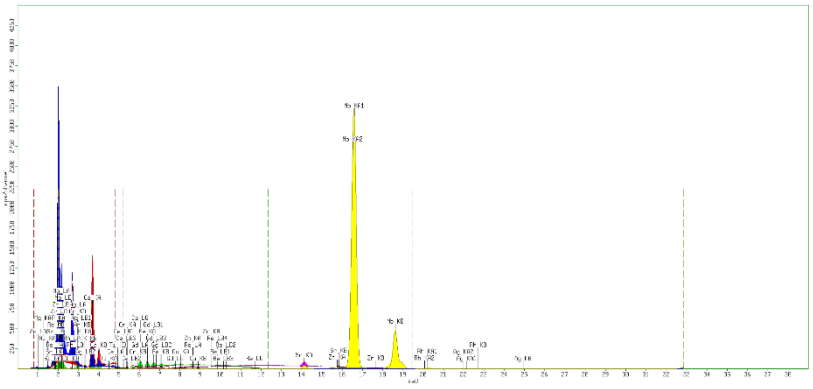

Fig. 12. The spectrum of x-ray fluorescence of triphosphate of Niobium NbP_3O_{10}

Table 5: Results of the XRF of NbP_3O_{10} phase

Compound	Conc	Unit
0Mg	324,7	ppm
Al	0,185	%
Si	0,595	%
P	**10,8**	**%**
Cl	0,387	%
K	922,8	ppm
Ca	6,168	%
Ti	202,2	ppm
Cr	226,5	ppm
Fe	0,119	%
Cu	172,9	ppm
Zn	201,3	ppm
Sr	0,135	%
Zr	391,7	ppm
Nb	**15,928**	**%**
Ag	0,135	%
Ce	331,9	Ppm
Gd	0,481	%
Re	18,3	ppm

III System Design, Mesh and Finite Element Modeling (FEM)

a) Industrial Design

In order to represent the mechanical characteristics of our implant, we drew on Catia V5 the real dimensions of an osteointegrated orthopedic implant.

The study of the mechanical resistance of our implant, in which we apply the new nanomaterial "triphosphate of niobium", is made by finite element modeling, by applying Von Mises constraints. The goal is to calculate the strain energy.

We applied an embedding on the base of the implant plus a compression loading on the other side which will be in contact with the prosthetic foot. the compressive force applied is of the order of 300 N/m2 (see figure 13)

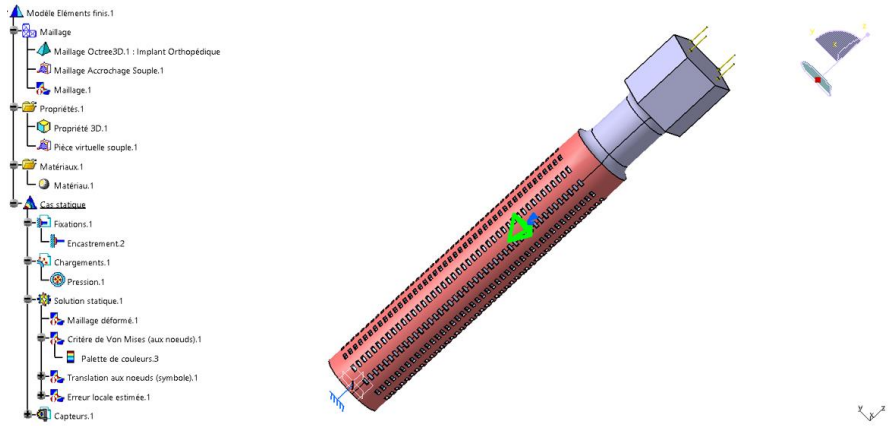

Fig. 13. Drawing of the sample to be characterized with mechanical compressions

Structure Calculation:

Number of nodes: 12208
Number of elements: 6480
Number of D.D.L: 36627
Number of contact relationships: 0
Number of kinematic relationships: 6
Number of coefficients: 339

b) Mesh

The mesh chosen is of fine size at the millimeter scale, also we applied parabolic elements to provide reliable results. The results of these parameters are given by the following figure 14.

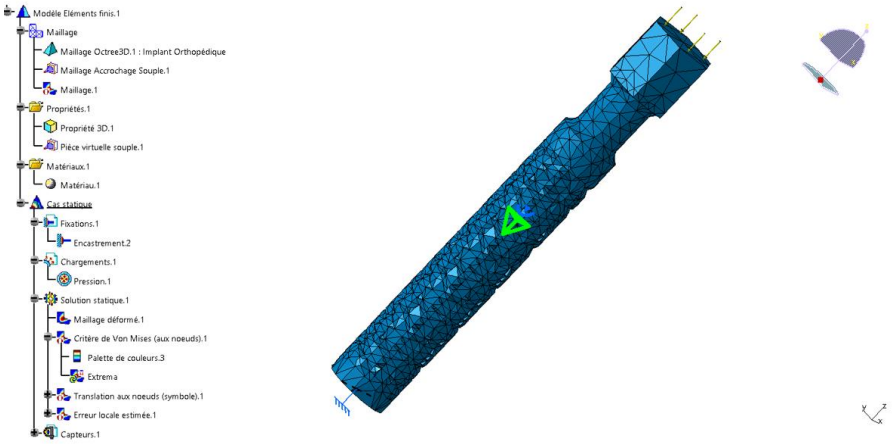

Fig. 14. Deformed mesh of our implant under mechanical loading

c) Finite Element Modeling (FEM): Von Mises Constraints

The Von Mises criterion is an energy criterion, it means the elastic strain energy, its mathematical formula in tension-compression is written:

$$U = \frac{1}{2}\sigma\varepsilon$$

σ: Constraint ; **ε:** Deformation or Relative elongation

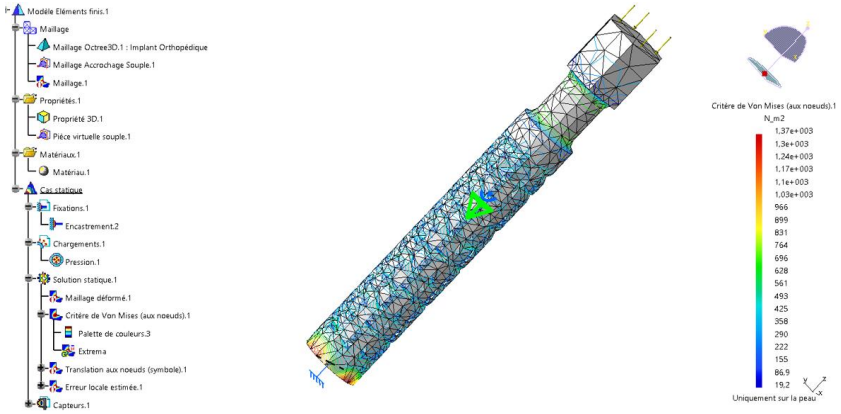

Fig. 15. Finite Element Modeling (FEM): Von Mises Constraints on Catia V5

Table 6: Balance Results

Components	Strengths Applied	Reactions	Residues	Error Relative
Fx (N)	1,02E-13	-7,62E-12	-7,52E-12	1,06E-09
Fy (N)	-1,08E-13	-7,99E-12	-8,10E-12	1,15E-09
Fz (N)	-1,04E+03	1,04E+03	2,26E-10	3,20E-08
Mx (Nxm)	1,48E-14	3,23E-13	3,38E-13	3,42E-10
My (Nxm)	1,52E-14	-3,91E-13	-3,76E-13	3,80E-10
Mz (Nxm)	2,83E-15	8,25E-14	8,53E-14	8,62E-11

Results

Strain energy (Implant with Triphosphate of Niobium NbP_3O_{10}) = 2.795e-011 J

Strain energy (Implant with Titanium) = 2.501e-011 J

Discussion

the results of our finite element modeling showed a difference in elastic strain energy between our nanomaterial "Triphosphate of Niobium NbP_3O_{10}" and pure titanium. Indeed, to deform an implant made of our alloy it is necessary to provide more energy in comparison with titanium. This shows that our nanomaterial improves the mechanical strength of the orthopedic implant.

Conclusion

Our New triphosphates of Niobium NbP_3O_{10} powder is prepared by a solid-state method. This sample is thermally treated at 1000°C for 6 h to get monazite type structure with orthorhombic system. The phase, nanomaterial and optical properties of triphosphates of Niobium sample is characterized by X-ray diffraction patterns, Fourier transform infrared spectra and fluorescence X (SFX). Unit cell parameters: a = 13.036 Å, b =11.3182 Å, c = 12.539(5) Å, $\alpha = \gamma = 90°$, $\beta = 117.903°$ and The mean crystallite size calculate from the XRD pattern has been found to be 0.04 µm. Fourier transform infrared spectra confirms the presence of characteristic bands from P_3O_{10} phosphate group.

Indeed, we have developed an identification map of our nanomaterial. these elements are potential for our second step which is the modeling of an orthopedic implant on CAD software, in order to verify these mechanical characteristics (Strain energy, Young's modulus, Poisson's ratio and its elastic limit). The objective is to compare the new nanomaterial with the titanium in order to validate our initial hypothesis, which is the improvement of the mechanical resistance.

References

1. P I Brånemark, B O Hansson, R Adell, U Breine, J Lindström, O Hallén AO. Osseointegrated implants in the treatment of the edentulous jaw. Experience from a 10-year period. Scand J Plast Reconstr Sug. 1977;16:1–132.
2. Schroeder, A.; Pohler, O.; Sutter F. Tissue reaction to an implant of a titanium hollow cylinder with a titanium surface spray layer. Schweizerische Monatsschrift fur Zahnheilkd. 1976;713–27.
3. Listgarten MA, Lang NP, Schroeder HE, Schroeder A. Periodontal tissues and their counterparts around endosseous implants. Clin Oral Implants Res [Internet]. 1991 Jul;2(3):1–19. Available from: http://doi.wiley.com/10.1034/j.1600-0501.1991.020309.x
4. Boyan BD, Cheng A, Olivares-Navarrete R, Schwartz Z. Implant Surface Design Regulates Mesenchymal Stem Cell Differentiation and Maturation. Adv Dent Res [Internet]. 2016 Mar 29;28(1):10–7. Available from: http://journals.sagepub.com/doi/10.1177/0022034515624444
5. Smeets R, Stadlinger B, Schwarz F, Beck-Broichsitter B, Jung O, Precht C, et al. Impact of Dental Implant Surface Modifications on Osseointegration. Biomed Res Int [Internet]. 2016;2016:1–16. Available from: http://www.hindawi.com/journals/bmri/2016/6285620/
6. Buser D, Broggini N, Wieland M, Schenk RK, Denzer AJ, Cochran DL, et al. Enhanced Bone Apposition to a Chemically Modified SLA Titanium Surface. J Dent Res [Internet]. 2004 Jul 20;83(7):529–33. Available from: http://journals.sagepub.com/doi/10.1177/154405910408300704
7. Zhao G, Schwartz Z, Wieland M, Rupp F, Geis-Gerstorfer J, Cochran DL, et al. High surface energy enhances cell response to titanium substrate microstructure. J Biomed Mater Res Part A [Internet]. 2005 Jul 1;74A(1):49–58. Available from: https://onlinelibrary.wiley.com/doi/10.1002/jbm.a.30320
8. Schwarz F, Herten M, Sager M, Wieland M, Dard M, Becker J. Histological and immunohistochemical analysis of initial and early subepithelial connective tissue attachment at chemically modified and conventional SLA®titanium implants. A pilot study in dogs. Clin Oral Investig [Internet]. 2007 Jul 31;11(3):245–55. Available from: http://link.springer.com/10.1007/s00784-007-0110-7
9. V. S. Vinila, Reenu Jacob, Anusha Mony, Harikrishnan G. Nair, Sheelakumari Issac, Sam Rajan, Anitha S. Nair, D. J. Satheesh JI. -Ray Diffraction Analysis of Nano Crystalline Ceramic PbBaTiO3. Cryst Struct Theory Appl. 2014;3.
10. Mohamed El Masloumia, c, Inhar Imaza,_ J-PC, Videaua J-J, Couzib M, Mesnaouic M, Mohamed Maazazc. Synthesis, crystal structure and vibrational spectra characterization of MI La(PO3)4 (MI ¼ Na, Ag). J Solid State Chem. 2005;178:3581–3588.
11. Krishna Bharat L, Jeon Y Il, Yu JS. Synthesis and luminescent properties of trivalent rare-earth (Eu3+, Tb3+) ions doped nanocrystalline AgLa(PO3)4 polyphosphates. J Alloys Compd [Internet]. 2014 Nov;614:443–7. Available from: https://linkinghub.elsevier.com/retrieve/pii/S0925838814014649
12. Dardar FE, Gross M, Krimi S, Couzi M, Lachgar A, Sebti S, et al. Synthesis, structural characterization and ionic conductivity of mixed alkali titanium phosphate glasses. Mediterr J Chem [Internet]. 2018 Dec 4;7(5):328–36. Available from: http://medjchem-v3.azurewebsites.net/index.php/medjchem/article/view/790